Acid–Base Characteristics of Bromophenol Blue–Citrate Buffer Systems in the Amorphous State

JINJIANG LI,[1] KOUSTUV CHATTERJEE,[2] ALES MEDEK,[2] EVGENYI SHALAEV,[2] GEORGE ZOGRAFI[1]

[1]School of Pharmacy, University of Wisconsin-Madison, Wisconsin 53705

[2]Groton Laboratories, Pfizer, Inc., Groton, Connecticut 06340

Received 14 May 2003; revised 22 September 2003; accepted 1 October 2003

ABSTRACT: In this study, we have examined the acid–base characteristics of various citrate buffer systems alone and in the presence of the pH indicator dye, bromophenol blue, in aqueous solution, and after lyophilization to produce amorphous material. Fourier transform Raman and solid-state nuclear magnetic resonance spectroscopy have been used to monitor the ratio of ionized to un-ionized citric acid under various conditions, as a function of initial pH in the range of 2.65–4.28. Ultraviolet–visible spectrophotometry was used to probe the extent of proton transfer of bromophenol blue in the citrate buffer systems in solution and the amorphous state. Spectroscopic studies indicated greater ionization of citric acid and bromophenol blue in solution and the solid state with increasing initial solution pH, as expected. Fourier transform Raman measurements indicated the same ratio of ionized to un-ionized citrate species in solution, frozen solution, and the amorphous state. It is shown that the ratio of species at any particular initial pH is primarily determined by the amount of sodium ion present so as to maintain electroneutrality and not necessarily to the fact that pH and pK_a remain unchanged during freezing and freeze drying. Indeed, for bromophenol blue, the relative ultraviolet–visible intensities for ionized and un-ionized species in the amorphous sample were different from those in solution indicating that the extent of protonation of bromophenol blue was significantly lower in the solid samples. It is concluded that under certain conditions there can be significant differences in the apparent hydrogen activity of molecules in amorphous systems. © 2004 Wiley-Liss, Inc. and the American Pharmacists Association J Pharm Sci 93:697–712, 2004

Keywords: amorphous; solid-state; acid–base equilibria; pH; lyophilization; glass transition; Raman spectroscopy; NMR

INTRODUCTION

The chemical instability of drugs is a major concern in the development of pharmaceutical products.[1] Although chemical instabilities generally occur more rapidly in solution, instability in the solid state often occurs, particularly at elevated temperatures and relative humidities.[1,2] Many drugs in the solid state will show chemical instability because of the presence of acidic or basic formulation components.[1–3] Gerhardt[4] and Bell and Labuza,[5] for example, have demonstrated the existence of a solid-state stability-pH profile which parallels, but is not identical to, that observed in solution. For lyophilized preparations, it has been shown that reactivity often is related to the initial solution pH, before lyophilization.[6–13] Recent studies of the cyclization of amorphous quinapril hydrochloride,

Jinjiang Li's present address is Boehringer Ingelheim Pharmaceuticals Co., Ridgefield, CT 06877.

Koustuv Chatterjee's present address is College of Pharmacy, University of Minnesota, MN 55455.

Correspondence to: George Zografi (Telephone: 608-262-2991; Fax: 608-262-5345;
E-mail: gdzografi@pharmacy.wisc.edu)

Journal of Pharmaceutical Sciences, Vol. 93, 697–712 (2004)

colyophilized with citric acid at different initial solution pH, have shown that initial pH, and the glass transition temperature, T_g, have an important role in affecting instability.[14] Evidence has been presented to show that, in some cases, the degree of ionization of acidic or basic groups appears to be retained from the initial solution to the final lyophilized solid; the term "pH memory" has been coined to describe this behavior.[15–17] In this context, an apparent "pH memory" effect also was observed for the inversion of sucrose in the amorphous solid state, in that the rate of chemical reactivity in the freeze-dried solid, that had identical chemical composition and T_g, correlated very well with the pH of the solution before freeze drying.[10] To study relationships between solution pH and properties of the resulting freeze-dried material, several different methods have been used. One approach uses spectroscopic methods, e.g., nuclear magnetic resonance (NMR) and infrared, that allow one to observe separate signals from ionized and nonionized forms of the same chemical species. For example, it has been shown, with NMR[18–20] and Fourier transform infrared[15] spectroscopic measurements, that the extent of protonation in freeze-dried polycrystalline samples of L-histidine,[18–20] and freeze-dried samples of tris(hydroxymethyl)aminomethane, glycine, and 3-hydroxybenzoic acid[15] was similar to the ionization state of the solution from which the freeze-dried solids were prepared. Based on these spectroscopic results, it also was suggested that the pK_a in solution and the apparent pK_a in the solid state were similar. This is an unexpected conclusion considering that removal of water from an aqueous solution of an organic solute can produce a significant change in the polarity of the system, from a polar aqueous solution with a relatively high dielectric constant to a less polar organic solid. In solutions, such changes in the dielectric constant of a system are usually accompanied by significant changes in the pK_a of ionizable groups. For example, for acetic acid, the pK_a increases from 4.76 in water to 10.32 in ethanol.[21,22] Similar changes have been noted for malonic and succinic acids.[21] Conversely, an amino group ($-NH_3^+/-NH_2$ equilibria) was shown to exhibit relatively minor changes in pK_a as a function of dielectric constant. That the local environment can alter the effective apparent pK_a of a solid system has also been demonstrated by hydrogen exchange,[23] and with pH indicator dyes.[24–27] In the case of indicator dyes, for example, changes of 0.5–2 units in the apparent pK_a of several indicators were reported when the indicators were adsorbed onto an Amberlite XAD-2 resin.[27]

It should be noted that the suggestion that pH and pK_a are similar in solution and in freeze-dried materials[15–20] is based on the observation that the extent of corresponding ionizable groups in solution and solid state were similar. However, this does not necessarily mean that pH and pK_a remain the same. For example, if the concentration of counterions is significantly higher than that of protons, the extent of ionization would mainly be dictated by the counterions in order to maintain electroneutrality; such counterion composition would not change upon freezing and freeze drying if a nonvolatile acid or base was used to control pH.

In this report, we have attempted to more systematically evaluate and compare some of the approaches described above, using a system containing a citric-citrate buffer lyophilized from solutions having various initial pH values. We have studied solutions and corresponding lyophilized amorphous solids, with particular attention to an estimation of the relative concentration of various un-ionized and ionized species. Three methods have been used to compare how they might indicate apparent acid/base properties in solution and in the solid state: Fourier transform (FT)Raman, NMR, and ultraviolet–visible (UV–vis) diffuse reflectance with a pH indicator dye probe. Use of NMR to measure ionization states in the solid state is well documented as discussed above. FTRaman was chosen because it is not very sensitive to water and allows one to avoid significant complications, which are often associated with the use of infrared for water-containing systems. Dye indicators previously have been used to compare "pH" values in aqueous solution and frozen aqueous solutions of the same composition.[24]

MATERIALS AND METHODS

Materials

Citric acid (monohydrate) was purchased from Mallinckrodt Chemical Co. (Paris, KY). Bromophenol blue, phenol, 4,4′-(1,1-dioxido-3*H*-2,1-benzoxathiol-3-ylidene)bis[2,6-dibromo-(9CI)] was obtained from Sigma-Aldrich Chemical Co. (Milwaukee, WI). Other chemicals used were all analytical grade. Deionized water was obtained using a SYBRON/Barnstead pressure cartridge purification system (Boston, MA).

Methods

Sample Preparation

For FTRaman measurements, aqueous solutions, frozen solutions, and amorphous samples of citric acid, having various initial solution pH values, were prepared in the following manner. Solution samples were prepared by first dissolving 2.1 g of citric acid monohydrate in deionized water in a 100-mL volumetric flask followed by addition of 1 N NaOH solution to adjust the solution pH to desired values. To prepare frozen solution samples, aqueous solutions of citric acid were quickly frozen by dipping solution-containing vials into liquid nitrogen. To prepare solid-state amorphous samples for FTRaman measurement, solution samples of various pH values were lyophilized using a commercial tray dryer (Dura-Stop; FTS Systems, Stone Ridge, NY) in combination with a condenser module (Dura-Dry-MP; FTS Systems). The vials used were liquid scintillation vials from Research Products International Co. (Mount Prospect, IL) with a volume of 20 mL (diameter 27–28 mm and height 57.5 mm). Solution samples were first transferred into scintillation vials, about 8 mL for each vial, followed by transferring the sample-containing vials to a freeze dryer, subsequently freezing to −40°C and then keeping the sample at this temperature for >24 h before applying vacuum of between 50 and 100 mT pressure. After 24 h under vacuum, the shelf temperature was raised to −30°C, −20°C, −10°C, and 0°C, respectively, every 12 h; secondary drying was performed at 25°C for 24 h. After lyophilization, samples were pulverized in a glove box under N_2 atmosphere followed by vacuum-oven drying at 25°C for 24 h. Samples for solution NMR measurements were prepared by dissolving lyophilized cakes (described below) in D_2O at a concentration of approximately 16 mg solid per mL (approximately 0.1 M citrate solution). Samples for solid-state NMR measurements were prepared by lyophilization of 0.1 M citrate solutions of various pH values using the procedure described below for samples measured by UV–vis diffuse reflectance.

Samples for the diffuse reflectance UV measurements were prepared as follows. Aqueous 0.1 M citrate solutions were prepared by titration of a solution of citric acid with a 10% w/v solution of sodium hydroxide at pH values of 2.98, 3.64, and 4.28. A stock solution of indicator, bromophenol blue, was prepared by dissolving 80 mg of indicator in 100 mL of deionized water. Stock solutions of bromophenol blue were added to 0.1 M citrate solutions with different pH values to reach a final indicator concentration of 0.02 mg/mL. A VirTis (Genesis) freeze dryer was used to lyophilize these aqueous solution samples. A type I borosilicate glass vial (20 mL, Wheaton) and a 20-mm flurotec coated D777-1 lyo-stopper (Daikyo) were used. The solution volume was 5 mL per vial. Samples were frozen in the lyophilizer using the following program: cooling to 5°C at 2°C/min, held for 30 min; cooling to −5°C at 2°C/min, held for 15 min; cooling at 1°C/min to −40°C, held for 30 min. The hold times were included to minimize the thermal lag between the shelf and the sample temperature. Primary drying was performed after heating from −40°C to −32°C at 0.5°C/min and holding at −32°C for 35 h at a pressure of 70 mT. For secondary drying, the samples were heated from −32°C to 30°C at 0.1°C/min and held at 30°C for 24 h. Samples were sealed in vacuum and crimped with an aluminum shell after taking them out of the freeze dryer to minimize any moisture uptake. In the final lyophilized samples, the weight ratio of citric acid to indicator was 960:1. Note, that two different freeze dryers were used to prepare samples for FTRaman and for the solid-state NMR and diffuse reflectance measurements because the study was performed at two different sites. In both cases, freeze drying produced completely amorphous cakes without collapse.

To ensure that lyophilization did not result in any pH changes in the reconstituted solution, all lyophilized samples were reconstituted with deionized water to the prelyophilization volume; and the pH of this solution was measured.

Exposure to Humidity

Selected lyophilized samples of citric acid from aqueous solutions of pH 2.98 and 4.28 were exposed to 56% relative humidity (RH) (saturated NaBr solution) in a constant temperature chamber at 25°C for >10 h to allow for water sorption equilibrium. Samples were removed periodically for FTRaman measurement. The water content after various times of exposure, measured using Karl Fischer titrimetry, ranged from 1.5 to 4.5% w/w.

Powder X-ray Diffraction (PXRD) and Optical Microscopic Analysis

The PXRD patterns of all lyophilized samples for FTRaman measurements were obtained at ambient temperature using a Scintag PadV powder

X-ray diffractometer (Scintag Inc., Santa Clara, CA) at 40 mA and 35 kV with Cu Kα radiation. Samples were transferred to a quartz sample holder and the scan range of 2θ was from 5° to 40°, with a step size of 0.02° and scanning rate of 5° min^{-1}. All samples were examined using an Olympus BH-2 optical microscope equipped with polarized light (Olympus Optical Co., Ltd., Tokyo, Japan); and no birefringence was observed. PXRD measurement of samples of NMR and diffuse UV reflectance studies were performed using a Siemens D 5005 X-ray diffractometer with an autosampling accessory. The lyophilized samples were scanned from 5° to 40° (2θ), with a step size of 0.03° and hold time of 1 s. PXRD measurements, performed at the two different sites, produced consistent results with amorphous materials. All lyophilized samples exhibited a broad halo centered at 2θ of approximately 19°; no sharp diffraction lines were observed.

Differential Scanning Calorimetry (DSC)

The DSC thermograms of lyophilized samples for measuring T_g were obtained using a Mettler 821e DSC (Mettler Instrument Inc., Cleveland, OH). The data acquisition was through an NT-based Mettler software program (STAR). Dry nitrogen gas was used as a purging gas at a flow rate of 120 mL per min. A Julabo FT 900 air cooler was used to cool the furnace. High purity indium was used for temperature calibration at a heating rate of 20 K per min. Typically, 5–10 mg of lyophilized sample was transferred to an aluminum pan in a glove box under N_2 atmosphere followed by sealing the pan nonhermetically. Measurement of T_g was performed by placing the sample pan with pinhole in a robotic sample plate followed by executing the program at a heating rate of 20 K per min. Two consecutive DSC experiments were performed for each sample. The T_g was determined as the extrapolated onset temperature using the second scan, after heating to 130°C.

Water Content Determination

Residual water contents of the freeze-dried samples used for solid-state FTRaman, NMR, and diffuse reflectance UV studies were measured by Karl Fischer coulometric titration using an Aquastar C-3000. Typically, samples were dissolved in Aquastar Single Coulomat Solution without opening vials, and then the solution was injected into the titration cell. All amorphous samples were found to have residual water contents in the range of 1.5–2.5% w/w.

pH Measurement

A Denver Instrument pH meter (model 225) equipped with a Fisher Scientific Accumet glass body pH electrode was used for pH measurements. The pH meter was calibrated using standard buffer solutions (Aldrich Chemical Co., Milwaukee, WI) of pH 1.00, 2.00, and 4.00 (±0.01).

FTRaman Measurement

FTRaman spectra were collected on a Bruker RFS 100 FTRaman system with a near infrared ND:YAG laser operating at 1064 nm. The laser power was typically 500 mW and a liquid nitrogen-cooled germanium detector was used. Backscattering radiation at an angle of 180° was collected, and the stokes scattering was reported. Five hundred scans over the wave number 250–4000 cm^{-1} at a resolution of 4 cm^{-1} were averaged for each sample. Typically, 100 mg of sample was placed in a vial and the vial was placed in the sample holder before collecting a spectrum. For frozen solution samples, the number of scans was significantly reduced to avoid melting of the ice. The scattering peak ratios of $-COO^-$ (1720 cm^{-1}) to $-COOH$ (1400 cm^{-1}) were calculated by integrating the scattering peak area for these two functional groups in FTRaman spectra.

NMR Measurement

For NMR measurement of solutions, dioxane was used as an internal reference standard. Citric acid solutions in D_2O were pipetted into an NMR tube followed by transfer of the sample tube into the NMR instrument. All solution NMR spectra were acquired on a Bruker 500 MHz Avance spectrometer.

For solid-state NMR measurement, 300 mg of sample was tightly packed into a 7-mm ZrO spinner for each sample analyzed. One-dimensional ^{13}C spectra were collected at ambient pressure using ^{1}H-^{13}C cross-polarization magic angle spinning (CPMAS) at 295 K on a Bruker 7 mm CPMAS probe positioned into a wide-bore Bruker Avance DSX 500 MHz NMR spectrometer. The samples were spun at 7000 Hz, corresponding to the maximum specified spinning rate for the 7-mm probe. The fast spinning speed minimized the intensities of the spinning side bands. To optimize the signal sensitivity, the cross-polarization contact time was adjusted to 1 ms. A total of 2048

scans were acquired, unless sensitivity limited, resulting in approximately 100 min acquisition times. The spectra were referenced using adamantane as an external standard with its upfield signal set to 29.5 ppm.

Solution and Diffuse Reflectance UV–Vis Measurement

For solution UV–vis measurements, aqueous solutions of citric acid, containing 0.02 mg/mL bromophenol blue, at various pH values were pipetted into a 5-mm cuvette followed by inserting the sample cell into a UV–vis instrument. A Unicam UV Series Spectrophotometer (Cambridge, UK) with Vision 32 software was used to obtain solution spectra. Typically, samples were scanned from 200 to 850 nm with a scan speed of 240 nm/s. For all measurements, a 4-nm slit width was used and data were collected at 1-nm intervals. All solution spectra were plotted as absorbance versus wavelength (nm). For diffuse reflectance measurements of lyophilized citric acid samples, the materials were first milled with a mortar and pestle in a glove box at <5% RH under nitrogen flow and packed into the sample holders under ambient RH followed by quickly transferring the sample holder to the UV–vis instrument. A Hewlett Packard 8453 UV–vis Spectrophotometer with a Labsphere Reflectance Spectroscopy Accessory and HP UV/vis Chemstation software was used. The system was calibrated with Spectralon standards. Circular powder cell holders fitted with a quartz plate were used. Typically, amorphous samples were scanned from 400 to 1000 nm with a scan speed of 240 nm/s. A 4-nm slit width was used and data were collected at 1-nm intervals. All spectra for freeze-dried materials were converted using the Kubelka-Munk model as shown below and plotting $F(R_\infty)$ against wavelength.[28]

$$F(R_\infty) = \frac{(1 - R_\infty)^2}{2R_\infty} \qquad (1)$$

where R_∞ is the fraction of incident light reflected by a sample.

RESULTS

Initial versus Reconstituted pH

In Table 1 are given values of pH for the various citric acid/citrate mixtures in solution before lyophilization and in the reconstituted solution after lyophilization. It can be seen that the solution pH values do not change significantly, indicating no loss of acidic or basic species present during lyophilization. In Table 2, we present the calculated composition of citric acid and mono- and dicitrate ions as well as the concentration ratio of $-COO^-$ to $-COOH$ at each pH, simply assuming the solution equilibria given in Scheme 1.

Table 1. Initial pH versus the pH of Reconstituted Solutions of Citric Acid after Lyophilization

Initial solution pH (±0.03)	Reconstituted pH (±0.03)
2.65	2.66
2.98	2.97
3.16	3.17
3.41	3.41
3.65	3.66
4.28	4.27

Values tabulated in Table 2 were calculated based on the following equations:

$$K_{a1} = \frac{[H^+][H_2Citrate^-]}{[H_3Citrate]}, \quad K_{a2} = \frac{[H^+][HCitrate^=]}{[H_2Citrate^-]}$$

$$K_{a3} = \frac{[H^+][Citrate^{---}]}{[HCitrate^=]}$$

For example, to calculate the fraction of citric acid in solution of a certain solution pH, the following equation was used:

$$\text{Citric acid} = \frac{1}{1 + K_{a1}/[H^+] + K_{a1}K_{a2}/[H^+]^2 + K_{a1}K_{a2}K_{a3}/[H^+]^3}$$

T_g's of Lyophilized Samples

In Table 3, we report the T_g's for the three species, citric acid, monosodium citrate, and disodium

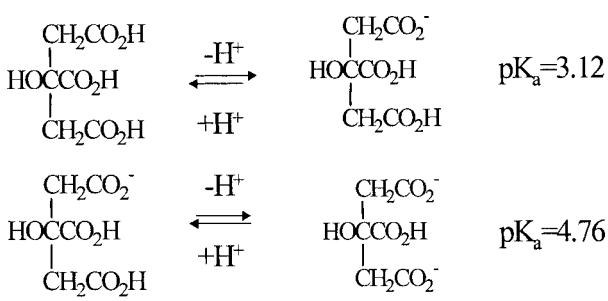

Scheme 1.

Table 2. Solution Composition of Citric Acid at Different pH Values Estimated from Solution Equilibria Shown in Scheme 1

Solution pH	Citric acid (% mole)	MonoCitrate (%)	DiCitrate (%)	TriCitrate	$\frac{-COO^-}{-COOH}$
2.65	75	25	—	0	0.091
2.98	58	42	—	0	0.16
3.16	47	52	1	0	0.22
3.40	33	64	3.0	0	0.30
3.65	21	73	6	0	0.40
4.28	5	70	23	2	0.68

citrate and for the amorphous samples obtained from lyophilization of solutions of varying initial pH. As expected, from individual T_g values and the species composition shown in Table 2, as the solution pH is increased, the T_g values of the lyophilized citric acid and citrate mixtures increase because of increased ionization.

FTRaman

Figure 1 contains a typical FTRaman spectrum of citric acid solution at pH 2.98. From the literature,[29] it can be shown that the scattering band around 3240 cm^{-1} is due to the stretching vibration of the $-OH$ group of citric acid, the band at $\sim$2947 cm^{-1} is due to the stretching vibration of $-CH_2$, and bands at $\sim$1720 cm^{-1} and $\sim$1400 cm^{-1} reflect the carbonyl stretching vibration of $-COO^-$ and $-COOH$. Scattering bands from 390 cm^{-1} to 1200 cm^{-1} are typically attributed to the C–C skeletal vibration; the band at 390 cm^{-1} is attributed to deformation of C–C and the rest of the bands are due to the stretching vibration of C–C. In this study, we are particularly interested in the region of 1200 cm^{-1} to 2000 cm^{-1} where the $-COO^-$ and $-COOH$ scattering bands are present, because $-COO^-$ and $-COOH$ are the functional groups of citric acid responsible for its acid–base characteristics.

Table 3. Glass Transition Temperatures, e.g., of Various Amorphous Samples Containing Citric Acid and Various Citrate Ions

Amorphous sample	T_g (°C)
Citric acid	11
NaCitrate	69
Na_2Citrate	115
Initial pH of 2.98	29
Initial pH of 3.40	43
Initial pH of 3.70	56
Initial pH of 4.28	66

Thus, the intensity ratio of these two scattering bands should represent their concentration ratio.

In Figure 2A, the FTRaman spectra of citric acid in solution in the region of 1200 cm^{-1} to 2000 cm^{-1} are shown as a function of solution pH, indicating that, as expected, the scattering intensity of $-COO^-$ relative to that of $-COOH$ increases with solution pH, whereas the scattering intensity of $-COOH$ relative to that of $-COO^-$ decreases with solution pH. Figure 2B presents the FTRaman spectra of citric acid at various solution pH values in the region of 1200 cm^{-1} to 2000 cm^{-1} after being converted to the frozen solution state; again, the scattering intensity of $-COO$ relative to that of $-COOH$ increases with solution pH whereas the scattering intensity of $-COOH$ relative to that of $-COO^-$ decreases with increasing solution pH; the signal to noise ratio is poor for the frozen solution, presumably because of the shorter acquisition time used to avoid the melting of ice (see Materials and Methods section). Figure 2C indicates that, as in the solution and frozen solution states, the

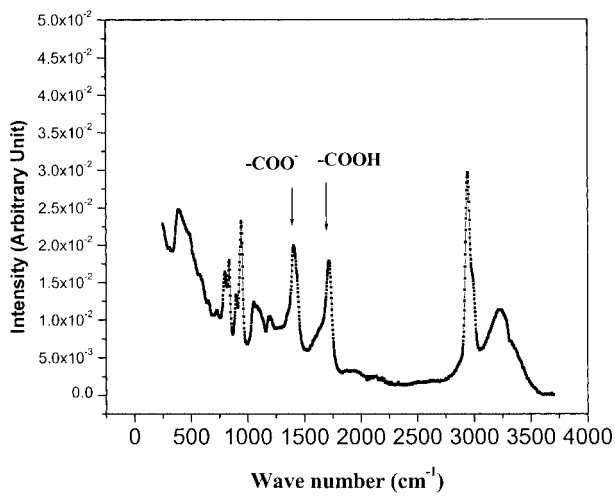

Figure 1. A typical FTRaman spectrum of citric acid in solution at pH 2.98.

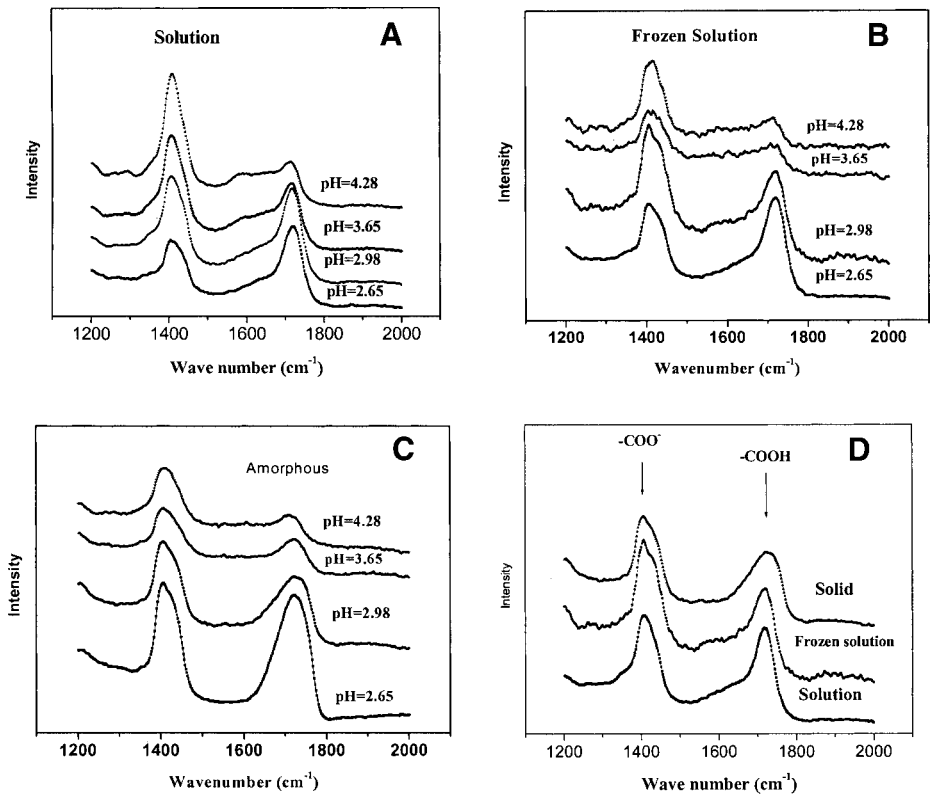

Figure 2. FTRaman spectra for citric acid in the region 1200 cm^{-1} to 2000 cm^{-1}: (A) solutions as a function of pH; (B) frozen solutions as a function of initial solution pH; (C) amorphous solids as a function of initial solution pH; (D) comparison of solution, frozen solution, and amorphous states from an initial pH of 2.98.

scattering intensity of $-COO^-$ in the amorphous state, relative to that of $-COOH$, increases with solution pH whereas the scattering intensity of COOH decreases with solution pH. Figure 2D displays the FTRaman spectra of citric acid at a solution pH of 2.98 in the region of 1200 cm^{-1} to 2000 cm^{-1} for the three states: aqueous solution, frozen solution, and the amorphous state together. Here, we see that the scattering bands of $-COO^-$ and $-COOH$ have similar peak shape and intensity for all three states, although the signal-to-noise ratio for $-COO^-$ and $-COOH$ in the frozen solution is higher than that obtained in aqueous solution and the amorphous state for the same reason mentioned above. Similar comparisons were made at other pH values (data not shown).

To quantitatively compare the acid–base characteristics of citric acid in all three states in the pH range studied, the scattering peak area ratio of $-COO^-$ (referred to in the following text as peak ratio) is plotted as a function of solution pH in Figure 3. Here, it can be seen that the increase of peak ratio with solution pH for all three states shows the same trend, although it can be noted that the peak ratios of $-COO^-$ to $-COOH$ in the amorphous or frozen solution states are slightly higher than those observed with the solution state in the higher pH range.

To evaluate the possible role of any residual water in the solid samples, lyophilized citrate samples were exposed to 56% RH for various lengths of time to give different levels of water content, from about 1.5% w/w to 4.5% w/w (see Materials and Methods section), followed by FTRaman measurements. In all cases, the peak ratio of $-COO^-$ to $-COOH$ remains essentially unchanged with time of exposure to water vapor (data not shown), and therefore we can conclude that the concentration ratio of $-COO^-$ to $-COOH$ remains the same in this range of water content, even though the activity of water is apparently changed by this process. This observation is consistent with the expectation that the ratio of ionized and un-ionized species is dictated only by the counterion composition (to be discussed).

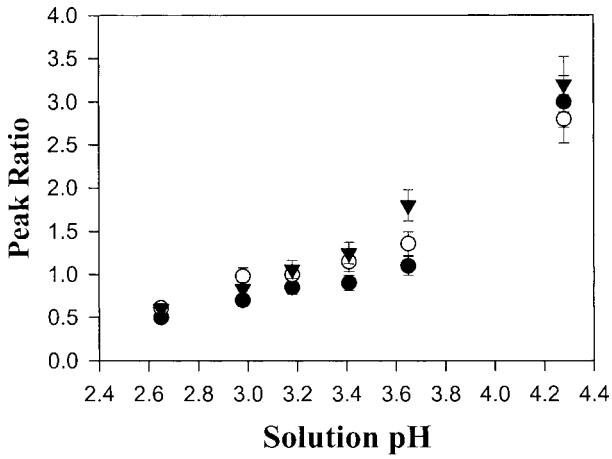

Figure 3. FTRaman peak intensity ratio of $-COO^-$ to $-COOH$ as a function of solution pH for three states: aqueous solution (●); frozen solution (○), and the amorphous state (▼).

NMR

Figure 4 contains ^{13}C solution NMR spectra of citric acid for various solution pH values ranging from 2.98 to 4.28. The peaks in Figure 4 can be assigned in the following manner (see Scheme 2). The methylene carbons (C3/5) of citric acid, which are degenerate and most shielded, have a chemical shift at ~44 ppm followed by the quaternary carbon (C4) that has a chemical shift at ~74 ppm. The two peaks at ~175 and ~178 ppm are attributed to carboxyl carbons, C2/6 and C8, respectively. Note that for both types of carboxyl carbons, single peaks were observed indicating a fast proton exchange on the NMR time scale. In this case, an observed chemical shift, δ_{av}, is determined by the chemical shifts (δ_i) of protonated and unprotonated species and their fraction, f_i

$$\delta_{av} = f_{COOH}\delta_{COOH} + f_{COO^-}\delta_{COO^-} \quad (2)$$

where δ_{av} is the chemical shift of the degenerate signal for either C2/6 or C8 carbon, f_{COOH} and f_{COO^-} are the molar fractions, and δ_{COOH} and δ_{COO^-} are the chemical shifts of the corresponding groups.

Figure 4 shows that the resonances of the carboxyl carbons are shifted downfield, i.e., become more de-shielded, as the solution pH increases. The downfield shift (i.e., increase in the chemical shift values) of the peaks of carboxyl carbons increases with increase in pH, as expected from Table 2. Methylene carbons and the ternary carbon exhibit the same trend, i.e., the chemical shift increases with pH. The magnitude of the change in the chemical shift is greater for the carboxyl carbon because it is directly affected by the charge density change resulting from ionization. The downfield shift with an increase in pH is consistent with an increased fraction of the more de-shielded group, $RCOO^-$. The chemical shift of

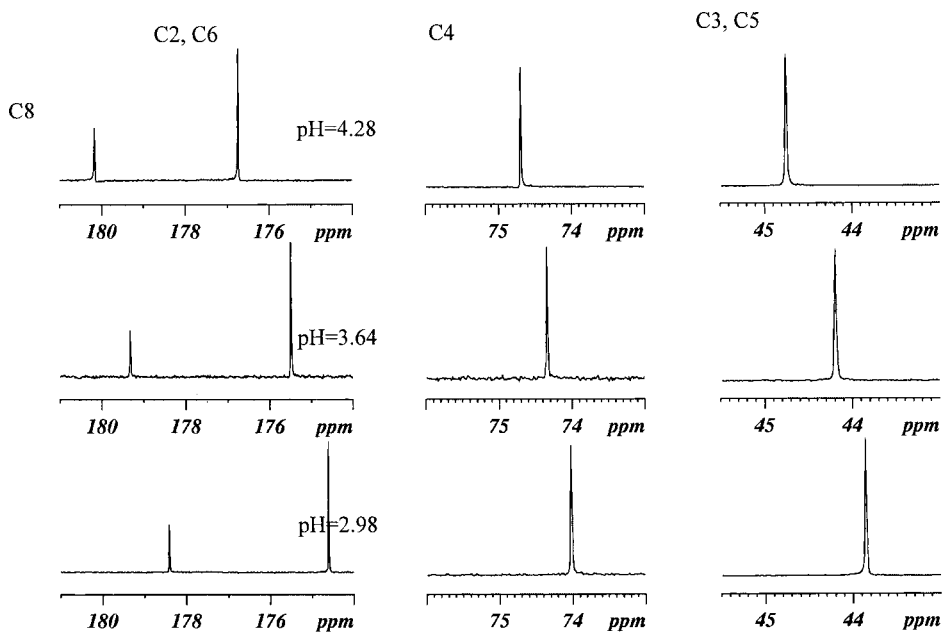

Figure 4. Solution ^{13}C NMR spectra of citric acid solutions with different pH values: from bottom to top, pH = 2.98, 3.64, and 4.28. See Scheme 2 for carbon atoms assignment.

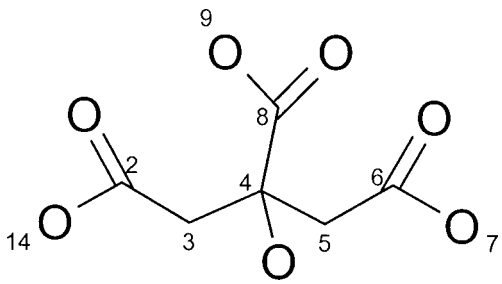

Scheme 2.

the carboxyl group increased by approximately 2 ppm as the pH was increased from 2.98 to 4.29. Changes in the chemical shifts for the methylene and quaternary carbons were less pronounced with an increase of <1 ppm.

Figure 5 presents the ^{13}C solid-state NMR spectra of citric acid samples lyophilized from aqueous solution of citric acid with corresponding solution pH values to those shown in Figure 4. In general, the spectra for amorphous citric acid display broader peaks than their solution counterpart, which is typical for amorphous samples. Assignment of the carbon resonances in the solid state is based on comparison with the known assignments from the corresponding solution state spectra, and is as follows: methylene carbons at ~44 ppm, quaternary carbon at ~74 ppm, and carboxyl carbon at ~177 ppm. In the freeze-dried samples, peaks for carboxyl carbons C2/6 and C8 (see Scheme 2 for atom assignment) were not resolved, and merged into one peak, likely because of peak broadening. In addition, separate signals for $-COOH$ and $-COO^-$ groups were not observed, also likely because of peak broadening. Similar to those in D_2O solution, ^{13}C resonances of lyophilized citric acid/citrate samples, shown in the ^{13}C solid-state spectra, are shifted downfield with increasing solution pH due to the de-shielding effect. The ^{13}C resonance for carboxyl carbon is shifted most with increasing solution pH, followed by the methylene and quaternary carbons.

Figure 6 shows chemical shifts of the carboxyl, methylene, and quaternary carbons as a function of pH in solution and the solid state. Chemical shifts for the ternary carbon (C4) and methylene carbons (C3, 5) in the solution were approximately 1 ppm lower than in the solid states. For carboxyl carbons (C2/6 and C8), direct comparison of solution and solid-state NMR results is not possible because two carboxyl peaks were observed in solution, whereas only one carboxyl peak was detected in the solid samples. To provide comparison for the

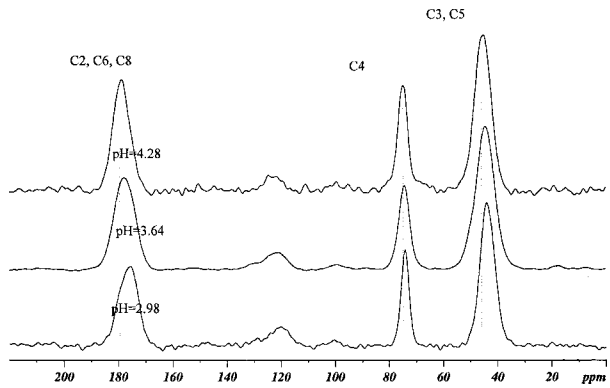

Figure 5. ^{13}C solid-state NMR spectra of samples lyophilized from solution with initial pH values: from bottom to top, pH 2.98, 3.64, and 4.28. See Scheme 2 for carbon atoms assignment. Broad peaks at approximately 105 and 125 ppm are spinning sidebands.

chemical shifts of carboxyl carbon in solution and solid state, average chemical shifts for carboxyl carbons in solution were calculated assuming a hypothetical situation whereby the C2,6 and C8 carbons degenerate [see eq. (2)].

$$\delta_{C2,6/8} = \left(2\delta_{C2,6} + \delta_{C8}\right)/3 \qquad (3)$$

where $\delta_{C2,6}$ and δ_{C8} are the chemical shifts of the C2,6 and C8 carbonyl carbons, respectively. In this calculation, we assume that the integral intensity (area) of an NMR peak is directly proportional to the number of corresponding carbons. The chemical shift of carboxyl carbons in solution calculated with an assumption that they are degenerate is shown in Figure 6 as a dotted line.

UV–Vis Spectroscopy Measurement

Figure 7 contains the solution UV–vis spectra of bromophenol blue in citric acid solutions of various pH values, as well as the diffuse reflectance spectra of bromophenol blue in the same region for samples lyophilized from the same aqueous solutions of citric acid. The absorption peaks of protonated and deprotonated components of bromophenol blue in solution can be located at 438 and 591 nm, respectively (Fig. 7A). Note in Scheme 3 that the terms "protonated" and "deprotonated" correspond to the second pK_a of bromophenol blue, and that the "protonated" form has one negative charge, InH^-, whereas the "deprotonated" has two negative charges, In^{2-}. In the solid state (Fig. 7B), the peaks are at 440 and 592 nm for InH^- and In^{2-}, respectively; this indicates that the position of the peaks did not

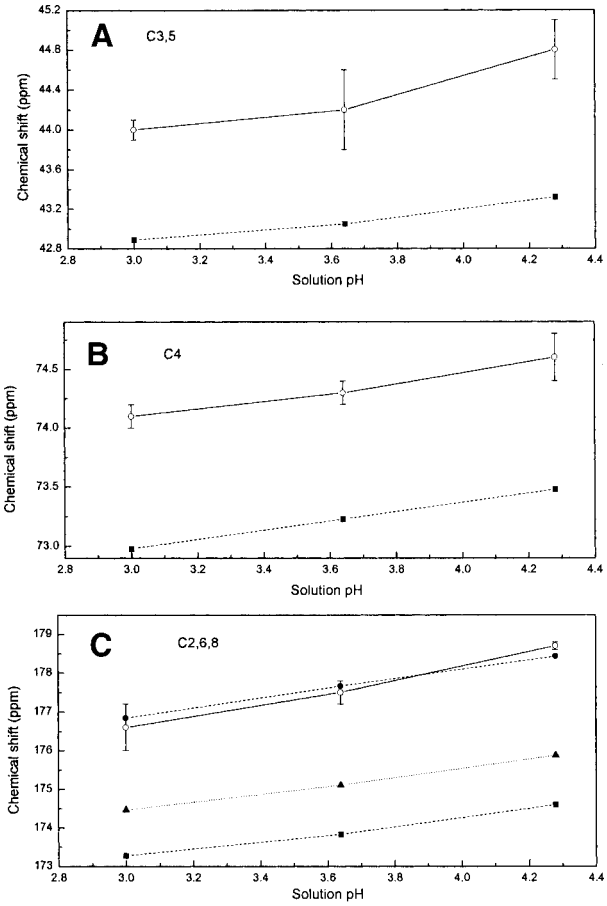

Figure 6. Chemical shift of ^{13}C of citric acid as a function of solution pH for methylene carbons C3,5 (A), ternary carbon C4 (B), and carboxylic carbons C2,6,8 (C): (■) solution, (○) amorphous freeze dried. On Figure 7C: (■) solution, C2,6 (●) solution, C8, (▲) average chemical shifts for C2,6,8 carboxyl carbons in solution calculated by assuming eq. (3) in text to be applicable.

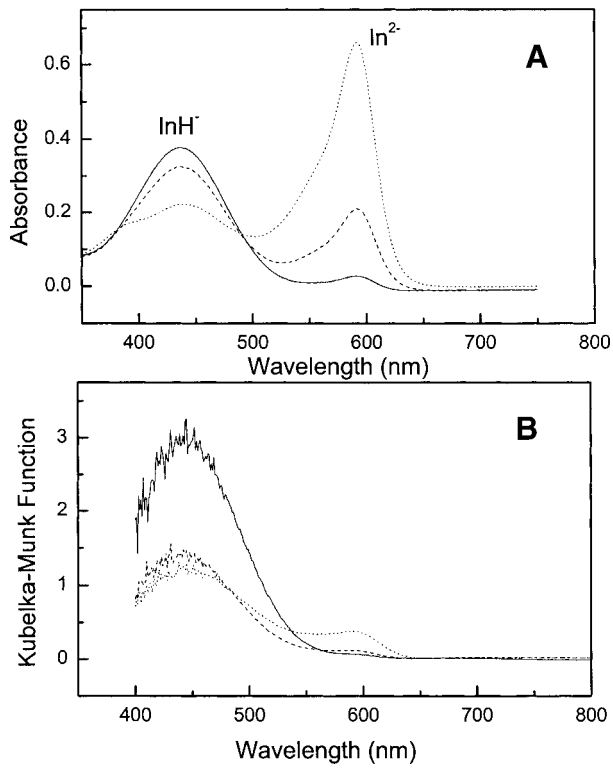

Figure 7. Visible absorbance spectra of bromophenol blue for aqueous solutions of citric acid at pH 2.98, 3.64, and 4.28 (A) and visible diffuse-reflectance spectra of their lyophilized counterpart (B). Solid, broken, and dotted lines correspond to samples at pH 2.98, 3.64, and 4.28, respectively. The peak with maximum absorption at 450 nm corresponds to the protonated form of the indicator (InH^-), and the peak with maximum absorption at 600 nm corresponds to the deprotonated form of the indicator (In^{2-}).

change significantly after freeze drying. Note that, for quantitative analysis, the peak intensities for solution samples are generally expressed as absorption, whereas the Kubelka-Munk function $F(R_\infty)$, as defined in the Materials and Methods section [eq. (1)], is used for solid samples. Figure 7 indicates that, as expected, the relative peak intensity for InH^- decreases with an increase in solution pH for both solution and solid-state spectra.

To compare the results for the solution and solid states, the peak ratios of In^{2-} to InH^- in the solution (r_l) and solid state (r_s) were calculated as follows:

$$r_1 = A_{In^{2-}}/A_{InH^-}, \qquad (4)$$

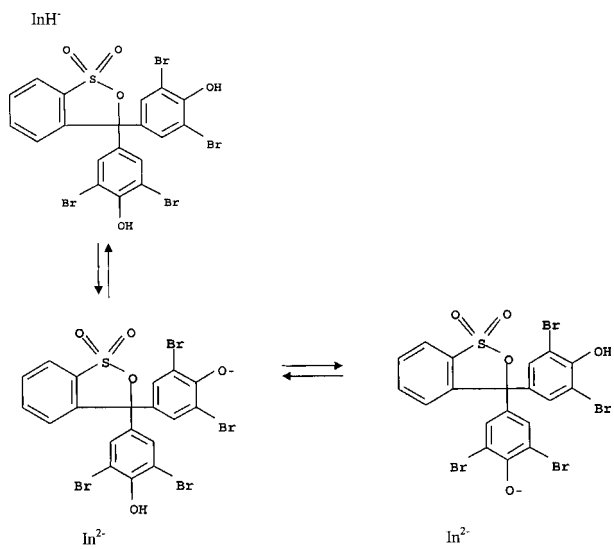

Scheme 3.

where r_l is the peak ratio in solution, and $A_{In^{2-}}$ and A_{InH^-} are the absorbance values of the deprotonated and protonated species, respectively.

$$R_s = F(R_\infty)_{In^{2-}}/F(R_\infty)_{InH^-}, \quad (5)$$

Where r_s is the peak ratio in the solid state, and $F(R_\infty)_{In^{2-}}$ and $F(R_\infty)_{InH^-}$ are the values of the Kubelka-Munk function of the deprotonated and protonated species, respectively.

The peak ratios for solution and solid samples are presented as a function of solution pH in Figure 8A, where it can be seen that the relative peak intensity of the deprotonated form of the indicator is significantly higher in the solution

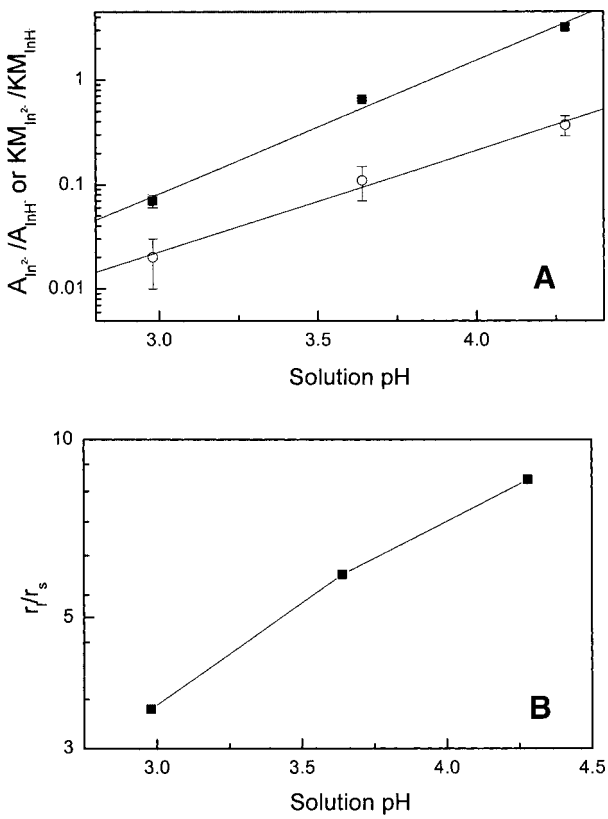

Figure 8. Comparison of the extent of protonation of bromophenol blue in solution and solid state. (A) Relationships between solution pH and ratio of spectral signals of deprotonated and protonated forms of bromophenol blue in solution, $r_1 = A_{In^{2-}}/A_{InH^-}$ (■) and solid state, $r_s = F(R_\infty)_{In^{2-}}/F(R_\infty)_{InH^-}$ (○). Lines are given as visual aid. (B) Difference in the extent of protonation of bromophenol blue in solution and in the solid state calculated from data represented in Figure 9A, using $r_l/r_s = (c_{In^{2-}}/c_{InH^-})^1/(c_{In^{2-}}/c_{InH^-})^s$, where c are concentrations of either protonated, InH^-, or unprotonated, In^{2-}, species of bromophenol blue in either solution, l, or solid state, s. See Results section, eqs. (4)–(9), for more detail. Lines are given as visual aid.

samples. This difference between solution and solid samples, expressed as r_l/r_s, increases with pH as shown in Figure 8B.

In solution, Beer's law is used to express relationships between concentration and the spectroscopic signal:

$$A = \log I_0/I = \varepsilon bc \quad (6)$$

where A is absorption, I_0 is the intensity of incident light, I is the intensity of transmitted light, ε is the molar extinction coefficient, b is path length which is constant under the specified experimental conditions, and c is concentration. Hence,

$$r_1 = A_{In^{2-}}/A_{InH^-} = (c_{In^{2-}}/c_{InH^-})^1(\varepsilon_{In^{2-}}/\varepsilon_{InH^-})^1 \quad (7)$$

In the solid state, relationships between the solid-state spectroscopic signal, i.e., Kubelka-Munk function, and concentration are expressed as[29]:

$$F(R_\infty) = (1-R_\infty)^2/2R_\infty = 2.303\ \varepsilon c/S \quad (8)$$

$$r_s = F(R_\infty)_{In^{2-}}/F(R_\infty)_{InH^-} = (c_{In^{2-}}/c_{InH^-})^s(\varepsilon_{In^{2-}}/\varepsilon_{InH^-})^s(S_{InH^-}/S_{In^{2-}}) \quad (9)$$

where S is equal to the scattering coefficient.

For relatively large particles, i.e., with the diameter much bigger than the wavelength of the incident radiation, scattering is independent of the wavelength.[29] Hence, scattering for the wavelengths that correspond to protonated and deprotonated species of the indicator, is the same, and $S_{InH^-}/S_{In^{2-}} = 1$. Hence, this consideration suggests that, if the extents of ionization of the indicator in solution and solid state, $(c_{In^{2-}}/c_{InH^-})^1$ and $(c_{In^{2-}}/c_{InH^-})^s$ are the same, the ratios of spectroscopic intensities, r_l and r_s, should be identical as well. It is not the case in this study as shown in Figure 8.

DISCUSSION

In this study, we have attempted to broaden our understanding of the nature of acid–base behavior in an amorphous solid, using the citric acid/citrate buffer system, and comparing results with those in corresponding aqueous solutions. Using techniques that are expected to be reflective of acid–base properties, i.e., FTRaman, NMR, and pH dye indicators, we have sought to observe the extent to which solution acid–base properties are altered

or remain the same in the solid state after lyophilization. We would expect FTRaman and NMR spectra to directly reflect the proton transfer that occurs between citric acid and its ionic forms, whereas the pH dye indicators would more directly reflect such proton transfer in the dye molecule, in response to the effects of the surrounding citric/citrate molecules. In this regard, the first two methods are different than the pH indicator method in that the former two methods monitor the buffer directly, whereas the dye indicator method monitors the indicator as it might be affected by the buffer. The dye indicator method has an additional potential value, however, in that the changes in spectra of the dye as affected by its environment would be expected to mimic the acid–base properties of a formulated amorphous drug in such a buffer matrix.

From the results obtained by FTRaman measurement, as shown in Figures 1–3, we can conclude that very similar changes in peak intensity ratios obtained from the spectra due to $-COO^-$ and $-COOH$ in the citric/citrate system, occur for the aqueous solutions, frozen solutions, and amorphous samples, despite the significant change in water content and its thermodynamic activity. For a more quantitative assessment of the ratio of concentrations of $-COO^-$ and $-COOH$ from the FTRaman results, we can use the following relationship between Raman scattering intensity (I_R) in watts and the number density of scatters (D), the cross-section laser intensity (I_0), the cross-section factor (σ_J), and the path length of the laser in the sample (dz).[29]

$$I_R = I_0 \sigma_J D dz \tag{10}$$

Assuming that I_0 and dz are constant for a given spectrometer, and σ_J is a molecular constant which is independent of a physical state of a sample, the scattering intensity (I_R) measured should primarily be affected by the concentration of molecules in the sample. Assuming further, that D is proportional to species concentration ([$-$COOH] and [$-COO^-$]), and S is the scattering coefficient for each functional group, which is proportional to I_0, σ_J, and dz in eq. (10), and A is the peak area of scattering intensity proportional to I_R, we can write a relationship between the area peak intensity, A, and the molar concentration of each species, where

$$\begin{aligned} A_{COOH} &= S_{COOH} \quad [-COOH] \\ \text{and } A_{COO^-} &= S_{COO^-}[-COO^-] \end{aligned} \tag{11}$$

Therefore, we can relate the peak ratio A_{COO^-}/A_{COOH} to concentration ratio as,

$$\frac{A_{COO^-}}{A_{COOH}} = C\frac{[-COO^-]}{[-COOH]} \tag{12}$$

where we assume that

$$C = \frac{S_{COO^-}}{S_{COOH}} \tag{13}$$

is a constant independent of the physical state of the sample.

To correlate the peak intensity ratio of functional groups ($-COO^-/-COOH$) to the molecular concentration of citric/citrate in the sample, the equilibrium of citric acid to form citrate in solution needs to be taken into consideration. For simplification, only the equilibrium for forming monocitrate is considered here (see Scheme 1) because at solution pH <3.70 little di-citrate forms in aqueous solution (see Table 2). Thus, the following relationship between molecular concentration of citric/NaCitrate, and concentrations of $-COO^-$ and $-COOH$ can be derived.

$$\begin{aligned} &[-COOH] = 3[H_3Citrate] + 2[H_2Citrate^-] \quad \text{and} \\ &[-COO^-] = [H_2Citrate^-] \end{aligned} \tag{14}$$

Therefore,

$$\begin{aligned} \frac{A_{COO}^-}{A_{-COOH}} &= C\frac{[-COO^-]}{[-COOH]} \\ &= C\frac{[H_2Citrate^-]}{3[H_3Citrate] + 2[H_2Citrate^-]} \\ &= C\frac{[H_2Citrate^-]/[H_3Citrate]}{3 + 2[H_2Citrate^-]/[H_3Citrate]} \end{aligned} \tag{15}$$

Eq. 15 shows that the peak intensity ratio of $-COO^-$ to $-COOH$ is a function of the degree of ionization ([$H_2Citrate^-$]/[$H_3Citrate$]), suggesting that if [A_{-COO^-}]/[A_{-COOH}] remains the same in aqueous solution, frozen solution, or the amorphous state, the degree of ionization of the carboxyl groups should be the same in all states.

We can further analyze our results in supporting this conclusion by replotting the data in Figure 3 in Figure 9 as log of peak ratio versus pH and comparing it to the log concentration ratios in solution versus pH calculated from the solution equilibria given in Scheme 1. Although the absolute values of $-COO^-/-COOH$ from peak ratios cannot be obtained without knowing the constant, C, we can see in Figure 9 a very similar relationship between [$-COO^-$]/[$-COOH$] and $A_{COO^-}/$

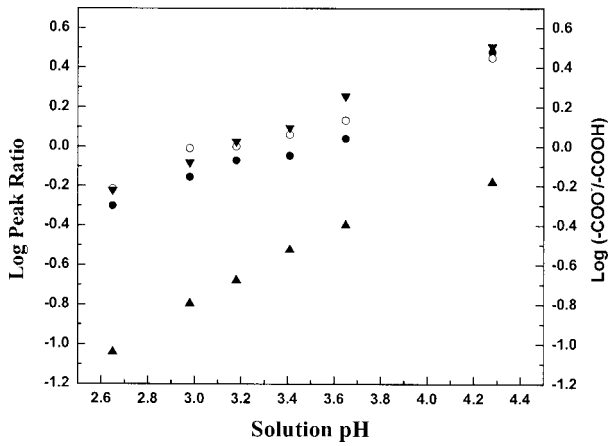

Figure 9. The logarithm of FTRaman peak intensity ratio versus initial solution pH for: aqueous solutions (●); frozen solutions (○); amorphous solids (▼). Logarithm of concentration ratios of $-COO^-$ to $-COOH$ calculated from solution equilibria data as in Scheme 1 (▲).

A_{COOH} (similar slope), and good agreement of A_{COO^-}/A_{COOH} for the three samples.

Using ^{13}C NMR measurements, it was not possible to directly determine the ratio of concentrations of $-COO^-$ to $-COOH$ because separate signals for protonated and nonprotonated species could not be obtained. However, the ^{13}C resonance for the carboxyl carbon relative to that for other carbons in D_2O solution and in the lyophilized sample are most significantly shifted downfield because of increasing de-shielding at higher initial solution pH; such parallel changes in the chemical shift with solution pH indicate that the ionization of carboxyl groups in the solid sample does depend on the initial solution pH.

It should be stressed that in cases reported in the literature, separate NMR peaks for ionized and non-ionized groups of histidine and imidazole were observed,[19,20] and the extent of ionization in such cases was directly determined from ratios of the intensities of corresponding peaks. Why, then, was this not observed for the citric acid/citrate systems? Because samples of histidine and imidazole, used in Refs. 19 and 20, appear to have been crystalline, the lack of resolution in this study might be explained by looking more closely at differences obtained between amorphous and crystalline samples of sodium citrate and citric acid. From these studies, it was observed that the half-width of the carboxyl peak in amorphous lyophilized samples was 8 ppm, whereas in crystalline samples of sodium citrate and citric acid (data are not shown) the half-widths were only 0.25 ppm for the carboxyl carbon. Thus, peak broadening could be preventing us from discerning differences between $-COO^-$ and $-COOH$. However, because it has been shown that in histidine, differences in chemical shifts between protonated and unprotonated carboxyls are >6 ppm in the solid state,[20] one might have expected to be able to observe separate peaks in the studied amorphous citrate samples, despite the relatively broad lines. In this regard, it should be mentioned that another possible reason for the degenerate $-COOH/-COO^-$ signal, that cannot be ruled out at this point, might be a fast proton exchange. Indeed, fast proton exchange in the solid state has been reported in several systems.[30–32] To determine whether or not the lack of resolution between NMR peaks in the freeze-dried amorphous samples occurs because of fast proton exchange, studies at low temperatures would have to be performed.

As mentioned above, pH indicator dyes in the solid state have been used to obtain some measure of acidity or basicity in frozen solution,[24] and the surface acidity of solid excipients and other solids.[25–27] As opposed to FTRaman and NMR, where we are observing responses due to the proportion of $-COO^-$ and $-COOH$ present, with the indicators we are observing absorbance changes due to proton transfer in the indicator itself, as influenced by the citric acid/citrate buffer matrix with which it has formed an amorphous molecular dispersion. As with the spectroscopic techniques, the response of the indicator in the solution and amorphous states does indicate a greater degree of ionization with increasing solution pH, as expected (see Fig. 9). This is an important observation because it clearly shows that a buffer system in the amorphous solid state, i.e., citric/citrate, can continue to impact directly on another ionizable molecule dispersed in the solid after lyophilization, even at very low levels of residual water content. However, the relative intensity of the signals of ionized species in the solid state was significantly lower than in solution. This observation implies that the extent of ionization of the indicator in the solid state is significantly lower than in solution, if we assume that the ratios of the extinction coefficients of ionized/non-ionized species in solution and solid state are the same. A lower extent of ionization of the indicator in the solid state might be expected if one considers that the polarity of a dehydrated sample is likely lower than that of the aqueous solution, e.g., the pK_a of bromophenol blue in solution should increase as the polarity of the medium decreases; for example,

the pK_a of bromophenol blue in water is 4.1, whereas in a medium of a lower polarity, methanol, it is 8.9.[33] We may note, therefore, that whereas FTRaman studies indicate the same extent of ionization in the solution and solid states, consistent with earlier Fourier transform infrared[15] and NMR[18–20] studies, this does not appear to be reflected in the observations made with the use of bromophenol blue as a "pH indicator."

To understand this apparent difference between the FTRaman for citric acid and the dye visible spectroscopy results, we must further consider issues related to the concentration or activity of all species, including protons. Let us first consider the apparent measurement of degree of ionization by Raman for the citric acid system. Any negative charges associated with $-COO^-$ groups in solution or as a solid must be compensated by an equal amount of positive charges to maintain electro-neutrality. Assuming that sodium ions (added during preparation of the initial solutions as sodium hydroxide) and hydrogen ions are the only positive charge species present, we may write:

$$[OH^-] + [-COO^-] \equiv [Na^+] + [H^+] \qquad (16)$$

In the pH range used here, $[OH^-]$ is very small and can be neglected, and therefore,

$$[-COO^-] = [Na^+] + [H^+] \qquad (17)$$

Thus, in principle, if we know the amount of Na^+ present and can estimate the amount of $-COO^-$ present, we can estimate $[H^+]$. We may note, however, that the molar concentration of sodium ions in the various preparations used in this study is much higher than that of protons for all pH values studied. For example, in 0.1 M citrate buffer at pH 2.98, the molar concentration of $[-COO^-]$ associated with $[Na^+]$ is approximately 0.05 M, whereas that of protons is approximately 0.001 M. Hence, we can see that the extent of ionization of citric acid is determined predominately by $[Na^+]$ that are present. Furthermore, although the concentration of protons $[H^+]$ in theory can be determined by the difference between $[-COOH^-]$ and [Na+] allowing us to estimate an approximate $[H^+]$ in the solid, $[H^+]$ is so significantly less in the pH range of interest that experimental measurements of $[-COO^-]$ and $[Na^+]$ may not be sensitive enough to provide accurate values. In this regard, FTRaman and other results shown in this article only confirm one aspect of the "pH memory effect," i.e., similarity in extent of ionization of a buffer in the solution and solid states. What this means is that the observed equivalence of $[-COO^-]$ and [−COOH] in the solution and solid state may or may not mean that hydrogen ion activity is the same in these two states.

Conversely, when using a dye indicator where dye concentrations are quite low, e.g., on the order of 10^{-5} M, the concentration of the dye is quite comparable to that of $[H^+]$. Hence, one would expect that the extent of ionization of the dye molecule would better reflect the proton donating/accepting ability of the matrix, i.e., "pH." Indeed, the use of pH indicators is generally accepted as a means of measuring acidity and basicity in a wide range of systems, from dilute aqueous or nonaqueous solutions to very concentrated aqueous solutions.[34] In this study, therefore, the fact that the ionization of the indicator in the citric/citrate aqueous solution was significantly higher than that in the solid citric/citrate system seems to more correctly indicate that one may expect significant differences in the ionization state of a drug molecule between solution and solid states under such conditions. However, changes in ionization of any particular molecule that is present at a low concentration cannot be quantitatively predicted from measurements for one probe molecule, bromophenol blue. The change in the ionization state of a drug that is present in a low concentration upon drying would depend on the chemical nature of the ionized and non-ionized species, as well as the properties of the matrix.

CONCLUSIONS

It appears from this work that we can distinguish two scenarios with respect to acid–base behavior of a drug molecule in amorphous solids relative to that in aqueous solution: 1) if a drug or excipient itself serves as a buffer, one can expect the possibility of similar extents of ionization in solution and solid states, as shown in this study by the FTRaman results. Such extents of ionization would primarily be dictated by the concentration of counterions and the requirement of electroneutrality. In such a case, for example, a reaction rate would depend on the state of ionization, and one might expect parallel pH dependence in solid and solution state reaction rates. 2) If a drug is present in relatively low amounts with respect to the concentration of a buffer that is present, as in the dye indicator studies, pH-stability profiles in solution and the solid state might be significantly

different, as was shown earlier in the case of the kinetics of degradation of peptides in buffered solution and solid states.[5,8]

ACKNOWLEDGMENTS

Partial financial support from the Purdue/Wisconsin Program on the Physical and Chemical Stability of Pharmaceutical Solids is gratefully acknowledged. The study was supported in part by a Pfizer Pharmaceutical Research and Development Summer Internship provided to K. C.

REFERENCES

1. Carstensen JT. 2000. Drug stability: Principles and practices, 3rd. ed. New York: Marcel Dekker.
2. Byrn SR, Xu W, Newman AW. 2001. Chemical reactivity in solid-state pharmaceuticals: Formulation implications. Adv Drug Deliv Rev 48:115–136.
3. Lai MC, Topp EM. 1999. Solid-state chemical stability of proteins and peptides. J Pharm Sci 88: 489–499.
4. Gerhardt A. 1990. Decomposition of phenobarbital in the solid state [PhD thesis]. University of Wisconsin-Madison, p 61.
5. Bell LN, Labuza TP. 1991. Aspartame degradation kinetics as affected by pH in intermediate and low moisture food systems. J Food Sci 56:17–20.
6. Lam XM, Costantino HR, Overcashier DE, Nguyen TH, Hsu C. 1996. Replacing succinate with glycolate buffer improves the stability of lyophilized interferon. Int J Pharm 142:85–95.
7. Badawy SF, Williams RC, Gilbert DL. 1999. Effect of different acids nonsolid-state stability of an ester prodrug of a IIb/IIIa glycoprotein receptor antagonist. J Pharm Sci 88:428–433.
8. Song Y, Schowen RL, Borchardt RT, Topp EM. 2001. Effect of 'pH' on the rate of asparagines deamidation in polymeric formulations: 'pH'-rate profile. J Pharm Sci 90:141–156.
9. Strickley RG, Visor GC, Lin L, Gu L. 1989. Unexpected pH effect on the stability of moexipril lyophilized powder. Pharm Res 6:971–975.
10. Shalaev EY, Lu Q, Zografi G. 2000. Acid-catalyzed inversion of sucrose in the amorphous state at very low levels of residual water. Pharm Res 17:366–370.
11. Guo Y, Byrn SR, Zografi G. 2000. Effects of lyophilization on the physical characteristics and chemical stability of amorphous quinapril hydrochloride. Pharm Res 17:930–935.
12. Strickley RG, Anderson BD. 1997. Solid-state stability of human insulin. II. Effect of water on reactive intermediate partitioning in lyophiles from pH 2–5 solutions: Stabilization against covalent dimer formation. J Pharm Sci 86:645–653.
13. Oliyai C, Patel JP, Carr L, Borchardt RT. 1994. Solid-state chemical instability of an asparaginyl residue in a model hexapeptide. J Pharm Sci Technol 48:167–173.
14. Li J, Guo Y, Zografi G. 2002. Effect of a citrate buffer system on the solid-state chemical stability of lyophilized quinapril preparations. Pharm Res 19:20–26.
15. Costantino HR, Griebenow K, Langer R, Klibnov AM. 1997. On the pH memory of lyophilized compounds containing protein functional groups. Biotech Bioeng 53:345–348.
16. Zacharis E, Halling PJ, Rees DG. 1999. Volatile buffers can override the "pH memory" of subtilisin catalysis in organic media. Proc Natl Acad Sci USA 96:1201–1205.
17. Vakos HL, Kaplan H, Black B, Dawson B, Hefford MA. 2000. Use of the pH memory effect in lyophilized proteins to achieve preferential methylation of α-amino groups. J Prot Chem 19(3):231–237.
18. Frey MH, Opella SJ. 1986. The effect of pH on the solid-state ^{13}C NMR spectra of histidine. J Magn Reson 66:144–147.
19. Munowitz M, Bachovchin WW, Herzfeld J, Dobson CM, Griffin RG. 1982. Acid-base and tautomeric equilibria in the solid state: ^{15}N NMR spectroscopy of histidine and imidazole. J Am Chem Soc 104: 1192–1196.
20. Henry B, Tekely P, Delpuech JJ. 2002. pH and pK determinations by high-resolution solid-state ^{13}C NMR: Acid-base and tautomeric equilibria of lyophilized 1-histidine. J Am Chem Soc 124(9):2025–2034.
21. Huang T-H, Bachovchin WW, Griffin RG, Dobson CM. 1984. High Resolution nitrogen-15 nuclear magnetic resonance studies of α-lytic protease in the solid state, direct comparison of enzyme structure in solution and in the solid state. Biochemistry 23:5933–5937.
22. Reichardt C. 1990. Solvents and solvent effects in organic chemistry. New York: VCH.
23. Careri G. 1998. Cooperative charge fluctuations by migrating protons in globular proteins. Progr Biophys Mol Biol 79:223–249.
24. Orii Y, Morita M. 1977. Measurement of the pH frozen buffer solutions by using pH indicators. J Biochem 81:163–168.
25. Glombitza BW, Oelkrug D, Schmidt PC. 1994. Surface acidity of solid pharmaceutical excipients. I. Determination of the surface acidity. Eur J Pharm Biopharm 40:289–293.
26. Glombitza BW, Schmidt PC. 1995. Surface acidity of solid pharmaceutical excipients. II. Effect of the surface acidity on the decomposition rate of acetylsalicylic acid. Eur J Pharm Biopharm 41:114–199.
27. Narayanaswamy R, Sevilla F III. 1986. Reflectrometric study of the acid–base equilibria of

indicators immobilized on a styrene/divinylbenzene copolymer. Anal Chim Acta 189:365–369.
28. Wendlandt WW, Hecht HG. 1966. Reflectance spectroscopy. New York: Interscience Publishers.
29. Lin-Ven D, Colthup NB, Fateley WG, Grasselli JG. 1991. The handbook of infrared and Raman characteristic frequencies of organic molecules. New York: Academic Press.
30. Toda F, Tanaka K, Foces-Foces C, Llamas-Saiz AL, Limbach H-H, Aguilar-Parrilla F, Claramunt RM, Lopez C, Elguero J. 1993. Intermolecular proton transfer in host-guest crystals: The case of pyrazole included in 1,1-Di(2,4-dimethylphenyl)but-2-yn-1-Ol, and X-ray and solid-state $^{13}C/^{15}N$ NMR study. J Chem Commun 1139–1142.
31. McGrego AC, Lukes PJ, Osman JR, Crayston JA. 1995. ^{13}C CP/MAS NMR studies of tetraazzaannulenes: Fast proton transfer in the solid state. J Chem Soc Perkin Trans 2:809–813.
32. Llamas-Saiz AL, Foces-Foces C, Fontenas C, Jagerovic N, Elguero J. 1999. The search for proton mobility in solid pyrazoles: Molecular and crystal structure of 3(5)-phenyl-4-bromo-5(3)-methylpyrazole. J Mol Struct 484:197–205.
33. Bates RG. 1973. Determination of pH. Theory and practice, 2nd ed. New York: John Wiley & Sons, p 156.
34. Bates RG. 1973. Determination of pH. Theory and practice, 2nd ed. New York: John Wiley & Sons, p 165.